Stable Adaptive Method to Solve FEM Coupled With Jiles–Atherton Hysteresis Model

Lauri Perkkiö[1], Brijesh Upadhaya[2], Antti Hannukainen[1], and Paavo Rasilo[2,3]

[1]Department of Mathematics and Systems Analysis, Aalto University, 00076 Espoo, Finland
[2]Department of Electrical Engineering and Automation, Aalto University, 00076 Espoo, Finland
[3]Department of Electrical Engineering, Tampere University of Technology, 33101 Tampere, Finland

The Jiles–Atherton magnetic hysteresis model coupled with time-stepping finite-element analysis is reported to suffer from numerical convergence problems, for example, when simulating electrical machines. In this paper, we describe a source of the numerical difficulties, and present a more stable time integration scheme for the coupled problem. In addition, we introduce the quasi-Newton method to accelerate the solution of the nonlinear field equation. Induction motor simulations verify the robustness of the proposed method.

Index Terms— **Finite-element method (FEM), Jiles–Atherton (JA), numerical methods, quasi-Newton (QN).**

I. Introduction

COMBINING the Jiles–Atherton (JA) magnetic hysteresis model [1] with time-stepping finite-element (FE) analysis is reported to suffer from numerical convergence problems, for example, when simulating the electromagnetic field in a transformer [2], [3]. The combined model involves coupling a differential $\partial \boldsymbol{H}/\partial \boldsymbol{B}$-constitutive relation with low-frequency Maxwell equations for the field strength $\boldsymbol{H}$ and flux density $\boldsymbol{B}$, and this is nontrivial both numerically [3] and mathematically [4]. Numerically, there are issues with slow or nonexistent convergence when the nonlinear equations are solved iteratively on each time step. More severely, the solution itself may blow up, meaning that the H–B curves eventually drift away from the true solution. This paper focuses on the numerical difficulties of the coupled JA-finite-element method (FEM) problem. Other problems, such as parameter fitting, improved JA-model, and comparison to measurements, will be addressed in separate works. From a more theoretic point of view, it is still uncertain in what sense hysteretic partial differential equations (PDEs) have well-defined solutions [5], [6], and research on such a topic could be interesting.

The most important observation in this paper is that the numerical stability and convergence problems are mitigated when the JA-differential equation is solved accurately enough at each field-equation time step. The required step size for the JA-equation can be several times smaller than what is required to solve the field equation. Thus, we use "subdivided" time steps for the JA-equation, as is done in [2] and [7]. In addition, we observe that the required step size can vary considerably at different parts of the hysteresis loop. This suggests using an adaptive scheme to solve the constitutive differential relation, which automatically refines the step size at the critical regions. In our numerical tests, in which a realistic rotating induction machine with coupled circuit equations is simulated, the adaptive error control removes the convergence and stability problems of the coupled JA-FEM-problem. The required step size to solve the JA-equation can be very small, in the worst case of order 1/100 compared with the FEM-problem time step, so the efficiency of the JA-equation solver requires special attention.

A quasi-Newton (QN) method, namely a variant of sparse Broyden's method [8], is presented to accelerate the solution of the nonlinear equation arising from the coupled (hysteretic) FE and circuit equations. The method, which is customized to fit our particular problem, can offer a significant speedup compared with a straightforward fixed-point (FP) method.

Manuscript received September 22, 2017; revised November 13, 2017; accepted December 4, 2017. Corresponding author: L. Perkkiö (e-mail: lauri.perkkio@aalto.fi).

Color versions of one or more of the figures in this paper are available online at http://ieeexplore.ieee.org.

Digital Object Identifier 10.1109/TMAG.2017.2782214

II. Vector Jiles–Atherton Model

A. Definition

The 2-D vector (inverse) JA-model described in [9] is employed in this paper. In the JA-model, the constitutive relation between $\boldsymbol{H}$ and $\boldsymbol{B}$ is given as a differential equation

$$\frac{\partial \boldsymbol{H}}{\partial \boldsymbol{B}} = \boldsymbol{\nu}_{\mathrm{JA}}(\boldsymbol{B}, \boldsymbol{H}, \Delta \boldsymbol{H}) \tag{1}$$

where the 2×2 tensor $\boldsymbol{\nu}_{\mathrm{JA}}$ is called the differential reluctivity. The last argument is a short-hand notation $\Delta \boldsymbol{H} := \partial_t \boldsymbol{H}/|\partial_t \boldsymbol{H}|$, meaning that only the direction, not the rate, of the change of $\boldsymbol{H}$ is significant. Rate-dependent (i.e., dynamic) terms can also be included, but they are neglected here for brevity.

The function $\boldsymbol{\nu}_{\mathrm{JA}}(\boldsymbol{B}, \boldsymbol{H}, \Delta \boldsymbol{H})$ is defined as follows. The model involves five parameters $(m_{\mathrm{s}}, k, c, a, \alpha)$, which are determined from measured H–B curves for different materials. A physical derivation of the model and the meaning of the parameters can be found in [10]. The magnetization $\boldsymbol{M} = \nu_0 \boldsymbol{B} - \boldsymbol{H}$, where ν_0 is the vacuum reluctivity, is separated into irreversible and anhysteretic terms, $\boldsymbol{M} = c\boldsymbol{M}_{\mathrm{an}} + (1-c)\boldsymbol{M}_{\mathrm{ir}}$. The effective field is defined as $\boldsymbol{H}_{\mathrm{e}} := \boldsymbol{H} + \alpha \boldsymbol{M}$, and the anhysteretic magnetization is given by

$$\boldsymbol{M}_{\mathrm{an}}(\boldsymbol{H}_{\mathrm{e}}) = m_{\mathrm{s}} L\left(\frac{|\boldsymbol{H}_{\mathrm{e}}|}{a}\right)\frac{\boldsymbol{H}_{\mathrm{e}}}{|\boldsymbol{H}_{\mathrm{e}}|} \tag{2}$$

where $L(x) := \coth(x) - 1/x$ is the Langevin function; other functions, like splines, can also be used to get a better fit with the measurements [11]. The irreversible term is given by the differential relation

$$\frac{\partial \boldsymbol{M}_{\rm ir}}{\partial \boldsymbol{H}_{\rm e}} = \frac{|\boldsymbol{M}_{\rm an} - \boldsymbol{M}_{\rm ir}|}{k} \begin{bmatrix} H_{{\rm e},x}^2 & H_{{\rm e},x}H_{{\rm e},y} \\ H_{{\rm e},x}H_{{\rm e},y} & H_{{\rm e},y}^2 \end{bmatrix} \quad \text{if } \Delta \boldsymbol{H} \cdot (\boldsymbol{M}_{\rm an} - \boldsymbol{M}_{\rm ir}) > 0 \tag{3}$$

else $(\partial \boldsymbol{M}_{\rm ir}/\partial \boldsymbol{H}_{\rm e}) = 0$. The if-condition is a vector generalization of the assumption that the change is reversible when (H, B) is below the anhysteretic curve and ΔH is negative (and vice versa) (see Fig. 1). Then

$$\frac{\partial \boldsymbol{M}}{\partial \boldsymbol{H}} = (\boldsymbol{I} - \alpha \boldsymbol{\chi})^{-1} \boldsymbol{\chi} \tag{4}$$

where $\boldsymbol{I}$ is the identity matrix and $\boldsymbol{\chi} := c(\partial \boldsymbol{M}_{\rm an}/\partial \boldsymbol{H}_{\rm e}) + (1 - c)(\partial \boldsymbol{M}_{\rm ir}/\partial \boldsymbol{H}_{e})$. Finally, the desired equation is

$$\boldsymbol{\nu}_{\rm JA}(\boldsymbol{B}, \boldsymbol{H}, \Delta \boldsymbol{H}) = \left(\frac{\partial \boldsymbol{B}}{\partial \boldsymbol{H}}\right)^{-1} = \nu_0 \left(\boldsymbol{I} + \frac{\partial \boldsymbol{M}}{\partial \boldsymbol{H}}\right)^{-1}. \tag{5}$$

It should be kept in mind that certain JA-parameters can give negative $\boldsymbol{\nu}_{\rm JA}$ in the scalar case (and negative definite in the vector case) [12]. As $\boldsymbol{\nu}_{\rm JA}$ appears later on as the material parameter in the field equation, "bad" parameters could cause problems. For example, if the Langevin function with parameters $m_{\rm s}, a, \alpha$ is used as the anhysteretic magnetization, the parameters must satisfy $(\alpha m_{\rm s}/3\ a) < 1$ in order to the anhysteretic curve be monotonously increasing in the H–B plane, which is needed to keep $\boldsymbol{\nu}_{\rm JA}$ positive.

B. Proposed Numerical Integration of JA Equation

In the inverse JA model, $\boldsymbol{B}$ is the independent variable, which is convenient when the vector potential formulation $\boldsymbol{B} = \nabla \times \boldsymbol{A}$ is used to solve the field equation. The magnetizing field $\boldsymbol{H}$ is solved from the differential equation (1) numerically by an explicit method. Given $(\boldsymbol{H}_i, \Delta \boldsymbol{H}_i, \boldsymbol{B}_i, \boldsymbol{B}_{i+1})$, where i denotes the ith time step, the "$\boldsymbol{B}$-step" $\Delta \boldsymbol{B} := \boldsymbol{B}_{i+1} - \boldsymbol{B}_i$ is divided into s subintervals, because in our test problem, we need to integrate (1) using several times smaller $\Delta \boldsymbol{B}$ than what is required to solve the time-stepping FEM problem. For brevity, explicit Euler is used to integrate each subinterval in the following scheme; in the actual implementation, we use the fourth-order Runge–Kutta (RK4). To make the coupling to the field equation (Section III) clear, the scheme is written as follows.

INPUT $(\boldsymbol{B}_i, \boldsymbol{B}_{i+1}, \boldsymbol{H}_i, \Delta \boldsymbol{H}_{\rm start}, s)$.

$\Delta \boldsymbol{H}_0 = \Delta \boldsymbol{H}_{\rm start}$.

FOR $m = 1, \ldots, s$

$$\boldsymbol{\nu}_{{\rm JA},m} = \boldsymbol{\nu}_{\rm JA}\left(\boldsymbol{B}_{i+\frac{m-1}{s}}, \boldsymbol{H}_{i+\frac{m-1}{s}}, \Delta \boldsymbol{H}_{\frac{m-1}{s}}\right) \tag{6}$$

$$\Delta \boldsymbol{H}_{i+m/s} = \tfrac{1}{s} \boldsymbol{\nu}_{{\rm JA},m} \Delta \boldsymbol{B} \tag{7}$$

$$\boldsymbol{H}_{i+m/s} = \boldsymbol{H}_{i+\frac{m-1}{s}} + \Delta \boldsymbol{H}_{m/s}. \tag{8}$$

OUTPUT $(\boldsymbol{H}_{i+1})$.

Noninteger indices denote the values at "substeps," and they are not needed later. The average reluctivity

$$\hat{\boldsymbol{\nu}}_{\rm JA} := \frac{1}{s} \sum_{m=1}^{s} \boldsymbol{\nu}_{{\rm JA},m} \tag{9}$$

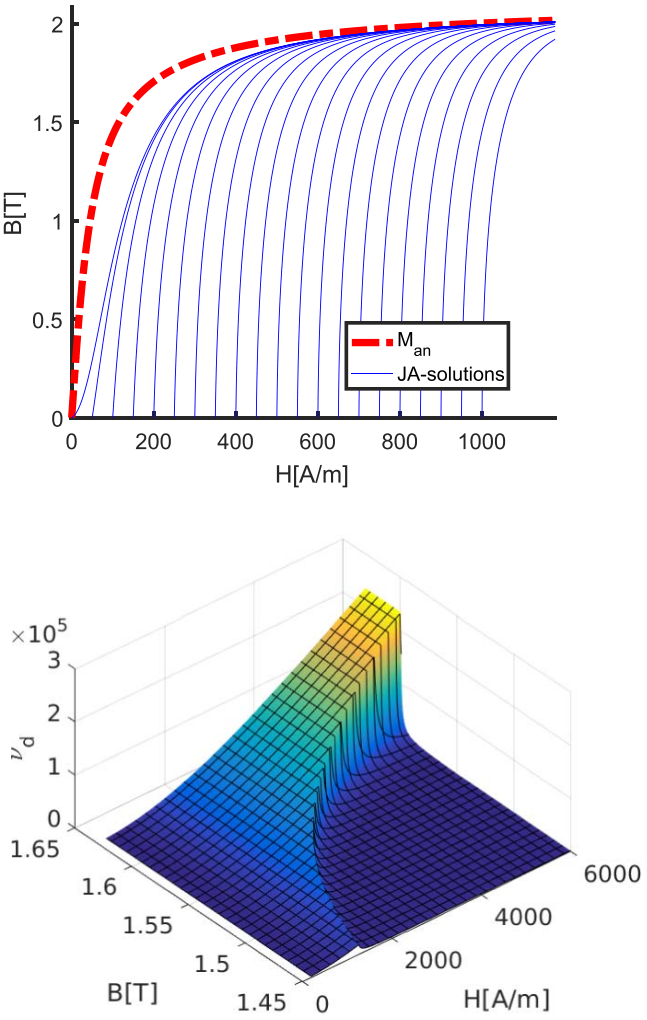

Fig. 1. Top: anhysteretic curve $M(H, B) = M_{\rm an}(H, B)$ in the H–B plane and some increasing $(\Delta H > 0)$ solutions to the scalar JA equation $dH/dB = \nu_{\rm d}(B, H, \Delta H)$ (implicitly defined). Bottom: Corresponding differential reluctivity $\nu_{\rm d}(B, H, \Delta H)$ in the H–B plane. Note that $\nu_{\rm d}$ varies rapidly close to the anhysteretic curve, which is an expected cause of numerical difficulties.

is stored for later use, because $\hat{\boldsymbol{\nu}}_{\rm JA}$ appears as a material parameter in the field equation in Section III. The resulting $\boldsymbol{H}_{i+1}$ can be expressed shortly as

$$\begin{aligned} \boldsymbol{H}_{i+1} &= \boldsymbol{H}_i + \sum_{m=1}^{s} \boldsymbol{\nu}_{{\rm JA},m} \frac{\boldsymbol{B}_{i+1} - \boldsymbol{B}_i}{s} \\ &= \boldsymbol{H}_i + \hat{\boldsymbol{\nu}}_{\rm JA}(\boldsymbol{B}_{i+1} - \boldsymbol{B}_i). \end{aligned} \tag{10}$$

The initial $\Delta \boldsymbol{H}$ can be chosen as $\Delta \boldsymbol{H}_{\rm start} = \boldsymbol{H}_i - \boldsymbol{H}_{i-1}$, but that leads to problems when an adaptive method is used (when the change switches from reversible to irreversible or vice versa [see (3)], this choice of $\Delta \boldsymbol{H}_{\rm start}$ forces the solution into the "wrong branch"). In our implementation, we first compute a candidate $\tilde{\boldsymbol{H}}_{i+1}$ by using explicit Euler without subdivisions $(s = 1)$, and use $\Delta \boldsymbol{H}_{\rm start} = \tilde{\boldsymbol{H}}_{i+1} - \boldsymbol{H}_i$ as the initial value for the actual RK4 solution.

The function $\boldsymbol{\nu}_{\mathrm{JA}}(\boldsymbol{B}, \boldsymbol{H}, \Delta\boldsymbol{H})$ is quickly varying near the anhysteretic curve $M = M_{\mathrm{an}}$ (or its equivalent hypersurface in the vector model) (see Fig. 1). Such rapid variation makes numerical integration more difficult. In addition, $\boldsymbol{\nu}_{\mathrm{JA}}$ is nondifferentiable on that curve [see (3)]. Also, the magnitude of $\boldsymbol{\nu}_{\mathrm{JA}}$ varies from small (close to B-axis) to large (at saturation region, large $\boldsymbol{B}$). These observations suggest using adaptive methods, such that different step sizes are used at different parts of the FE solution region. This is explained in Section V.

III. Coupled Field and JA Equations

Consider a magnetoquasi-static (i.e., low-frequency) field problem in domain Ω, where the currents flow in the z-direction and the $\boldsymbol{H}$ and $\boldsymbol{B}$ fields have only x- and y-components [13]. This is an adequate approximation to model, for instance, a cross section of a rotating electrical machine. In this 2-D approximation, the vector potential has only one component $\boldsymbol{A}(x, y) = A(x, y)\boldsymbol{e}_z$. The magnetic and electric fields are $\boldsymbol{B} = \nabla \times \boldsymbol{A}$ and $\boldsymbol{E} = -(\partial/\partial t)A$. The field $\boldsymbol{H}$ is governed by the PDE

$$\nabla \times \boldsymbol{H} = \boldsymbol{J} + \sigma \boldsymbol{E} \tag{11}$$

where $\boldsymbol{J} = J\boldsymbol{e}_z$ is an "imposed" current density (e.g., in stator windings) and σ is the electrical conductivity (nonzero in bulk conductors, e.g., rotor bars). The current density $\boldsymbol{J}$ may be coupled to external circuit equations, modeling, for example, three-phase stator windings, but coupling is omitted in these derivations for brevity (it is included in the numerical tests). The domain Ω is divided into hysteretic and non-hysteretic regions $\Omega = \mathrm{Fe} \cup \mathrm{N}$. The constitutive relation is $\boldsymbol{H} = \nu_0 \boldsymbol{B}$ in N and (1) in Fe. The Dirichlet boundary condition $A = 0$ is applied on the boundary $\partial\Omega$. To get the weak form of (11), the equation is multiplied by a test function $\boldsymbol{\phi} = \phi \boldsymbol{e}_z$, integrated over the domain Ω, and then partially integrated resulting in

$$\left(\sigma \tfrac{\partial}{\partial t} A, \phi\right)_\Omega = (J, \phi)_\Omega - (\boldsymbol{H}, \nabla \times \boldsymbol{\phi})_\Omega \tag{12}$$

where $(u, v)_\Omega$ denotes integration $\int_\Omega u \cdot v$ (and the boundary term vanishes due to the Dirichlet boundary condition). For simplicity, implicit Euler is applied for time discretization (one could also use Crank–Nicolson)

$$\begin{aligned}(\sigma A_{i+1}, \phi)_\Omega &= (\sigma A_i, \phi)_\Omega + \Delta t \left\{(J_{i+1}, \phi)_\Omega - (\boldsymbol{H}_{i+1}, \nabla \times \boldsymbol{\phi})_{\mathrm{N}}\right. \\ &\quad \left. - (\boldsymbol{H}_{i+1}, \nabla \times \boldsymbol{\phi})_{\mathrm{Fe}}\right\}. \end{aligned} \tag{13}$$

As $(\nabla \times (u\boldsymbol{e}_z), \nabla \times (v\boldsymbol{e}_z)) = (\nabla u, \nabla v)$, the nonhysteretic term is $(\boldsymbol{H}_{i+1}, \nabla \times \boldsymbol{\phi})_{\mathrm{N}} = (\nu_0 \nabla A_{i+1}, \nabla \phi)_{\mathrm{N}}$. In Fe, an integration method [see (9) and the preceding scheme]

$$\boldsymbol{H}_{i+1} = \boldsymbol{H}_i + \hat{\boldsymbol{\nu}}_{\mathrm{JA}}(\nabla \times \boldsymbol{A}_{i+1} - \nabla \times \boldsymbol{A}_i) \tag{14}$$

is applied, resulting in

$$\begin{aligned}(\boldsymbol{H}_{i+1}, \nabla \times \boldsymbol{\phi})_{\mathrm{Fe}} &= (\boldsymbol{H}_i, \nabla \times \boldsymbol{\phi})_{\mathrm{Fe}} + (\hat{\boldsymbol{\nu}}_{\mathrm{JA}} \nabla \times A_{i+1}, \nabla \times \boldsymbol{\phi})_{\mathrm{Fe}} \\ &\quad - (\hat{\boldsymbol{\nu}_{\mathrm{JA}}} \nabla \times A_i, \nabla \times \boldsymbol{\phi})_{\mathrm{Fe}}. \end{aligned} \tag{15}$$

Substituting this into (13), the weak form of the problem to be solved at each time step is the following: find potential $\boldsymbol{A}_{i+1} = A_{i+1}\boldsymbol{e}_z$ that satisfies

$$\begin{aligned}&(\sigma A_{i+1}, \phi) \\ &\quad + \Delta t \left\{(\nu_0 \nabla A_{i+1}, \nabla \phi)_{\mathrm{N}} + (\hat{\boldsymbol{\nu}}_{\mathrm{JA}} \nabla A_{i+1}, \nabla \phi)_{\mathrm{Fe}}\right\} = (\sigma A_i, \phi) \\ &\quad + \Delta t \left\{(J_{i+1}, \phi) - (\boldsymbol{H}_i, \nabla \times \boldsymbol{\phi})_{\mathrm{Fe}} + (\hat{\boldsymbol{\nu}}_{\mathrm{JA}} \nabla A_i, \nabla \phi)_{\mathrm{Fe}}\right\} \end{aligned} \tag{16}$$

for all test fields $\boldsymbol{\phi} = \phi \boldsymbol{e}_z$.

To discretize (16) spatially, the simplest option is to use linear elements for A, using three Gaussian quadrature points per element to integrate terms without gradient or curl and one quadrature point to evaluate the terms involving derivatives. The discretized $\boldsymbol{H}$ can be considered to be an elementwise constant vector field determined by (14) in each element, for example, with an initial condition $\boldsymbol{H}_0 = 0$. The test functions ϕ are the linear basis functions. Degrees of freedom (DoFs) for A_i are denoted by $\boldsymbol{a}_i$, and DoFs for $\boldsymbol{H}_i$ by $\boldsymbol{h}_i^x$ and $\boldsymbol{h}_i^y$. Thus, for linear elements, $\boldsymbol{a}_i \in \mathbb{R}^{\#\mathrm{nodes}}$ and $\boldsymbol{h}_i^x, \boldsymbol{h}_i^y \in \mathbb{R}^{\#\mathrm{Fe-triangles}}$. In each time step, the system of equations to be solved with respect to $\boldsymbol{a}_{i+1}$ is

$$\begin{aligned}&\{\boldsymbol{M} + \Delta t(\boldsymbol{K} + \boldsymbol{K}^{\mathrm{Fe}}(\boldsymbol{a}_{i+1}))\}\boldsymbol{a}_{i+1} \\ &\quad = \boldsymbol{M}\boldsymbol{a}_i + \Delta t(\boldsymbol{C}\boldsymbol{j}_{i+1} - \boldsymbol{D}^x \boldsymbol{h}_i^x - \boldsymbol{D}^y \boldsymbol{h}_i^y + \boldsymbol{K}^{\mathrm{Fe}}(\boldsymbol{a}_{i+1})\boldsymbol{a}_i) \end{aligned} \tag{17}$$

where Δt is the time step length, $\boldsymbol{M}_{k,l} := (\sigma\phi_k, \phi_l)$ is the mass matrix, $\boldsymbol{K}_{k,l} := (\nu_0 \nabla \times \phi_k, \nabla \times \phi_l)$ is the linear part of the stiffness matrix, $\boldsymbol{C}_{k,l} := (1/\mathrm{area}(S_l))(1, \phi_k)_{S_l}$ connects the source current $\boldsymbol{j}_l$ at phase l to the system, and $\boldsymbol{D}_{k,l}^x := (\partial_y \phi_k, 1)_{\mathrm{Fe}(l)}$, $\boldsymbol{D}_{k,l}^y := (-\partial_x \phi_k, 1)_{\mathrm{Fe}(l)}$, where $\mathrm{Fe}(l)$ is the lth iron element. The nonlinearity due to the JA model appears in the term

$$\boldsymbol{K}_{k,l}^{\mathrm{Fe}}(\boldsymbol{a}_{i+1}) = (\hat{\boldsymbol{\nu}}_{\mathrm{JA}}(\boldsymbol{a}_{i+1}) \nabla \phi_k, \nabla \phi_l)_{\mathrm{Fe}} \tag{18}$$

where $\hat{\boldsymbol{\nu}}_{\mathrm{JA}}$ depends on $\boldsymbol{a}_{i+1}$ through the numerical JA-equation solution [see (9)]. Matrices $\boldsymbol{M}, \boldsymbol{C}$, and $\boldsymbol{D}$ are fixed during simulation. If rotor motion is included (for example, by remeshing), certain elements of $\boldsymbol{K}$ will depend on the rotor position.

IV. Nonlinear Field-Equation Solution

To express the system of equations to be solved at each time step more formally, (17) is rewritten as

$$\boldsymbol{f}(\boldsymbol{x}) := \boldsymbol{A}(\boldsymbol{x})\boldsymbol{x} - \boldsymbol{b} = 0 \tag{19}$$

where $\boldsymbol{x} := \boldsymbol{a}_{i+1} - \boldsymbol{a}_i$ and

$$\boldsymbol{A}(\boldsymbol{x}) := \tfrac{1}{\Delta t}\boldsymbol{M} + (\boldsymbol{K} + \boldsymbol{K}^{\mathrm{Fe}}(\boldsymbol{x})) \tag{20}$$

$$\boldsymbol{b} := \boldsymbol{C}\boldsymbol{j}_{i+1} - \boldsymbol{D}\boldsymbol{h}_i - \boldsymbol{K}\boldsymbol{a}_i. \tag{21}$$

The unknown $\boldsymbol{x}$ is chosen as above, because $\boldsymbol{x} = \boldsymbol{a}_{i+1}$ would lead to $\boldsymbol{x}$-dependent load term $\boldsymbol{b}(\boldsymbol{x})$.

A. Fixed-Point Method

A straightforward method to solve (19) is the FP iteration

$$\boldsymbol{x}_{k+1} = \boldsymbol{A}(\boldsymbol{x}_k)^{-1}\boldsymbol{b} =: \boldsymbol{F}(\boldsymbol{x}_k). \tag{22}$$

This iteration is not guaranteed to converge for arbitrary parameters and initial guess $\boldsymbol{x}^0$. However, we expect convergence for small enough Δt and accurate enough JA solution by the following reasoning, which agrees with our numerical experiments. The convergence of iteration (22) depends on the smoothness of $\boldsymbol{F}$ with respect to $\boldsymbol{x}$. If there is a considerable error in JA-equation's integration, the function $\boldsymbol{F}$ will be less smooth, and the iteration converges more slowly, or not at all. This is seen in our numerical tests; choosing too large tolerance (29) leads to bad convergence.

The iteration (22) is called "the Newton–Raphson (NR) method" in [2] and [9], but we prefer to call it the FP method. What is called the Jacobian in [2] and [9] is actually the differential JA-model (1) itself. According to our understanding, the actual Jacobian is some complicated function depending on the chosen JA-integration scheme.

B. Sparse Broyden's Method

It is well known that the iteration (22) may converge slowly when a single-valued (SV) H–B curve is used [14], and the same can be observed with the JA model. To improve the convergence rate, a QN scheme is introduced as follows. The iteration to solve (19) is expressed in the form

$$\boldsymbol{x}_{k+1} = \boldsymbol{x}_k - [\boldsymbol{Q}(\boldsymbol{x}_k)]^{-1}\boldsymbol{f}(\boldsymbol{x}_k) \tag{23}$$

where $\boldsymbol{Q}$ depends on the chosen method. In the SV H–B case, it is often possible to compute the exact Jacobian $\boldsymbol{J}(\boldsymbol{x}) := D_{\boldsymbol{x}}\boldsymbol{f}(\boldsymbol{x})$, which results in the NR method. Another possibility is to choose $\boldsymbol{Q}^{-1} = \alpha\boldsymbol{A}^{-1}$, which is the FP method (22) with the relaxation parameter α. Computing the exact Jacobian is in practice impossible with the JA model, because $\partial_{\boldsymbol{x}_k}\hat{\boldsymbol{v}}_{\mathrm{JA}}(\boldsymbol{x})$ is a complicated function involving derivatives $\partial_{\boldsymbol{B}}\boldsymbol{v}_{\mathrm{JA}}$ and $\partial_{\boldsymbol{H}}\boldsymbol{v}_{\mathrm{JA}}$. Also, computing an approximate Jacobian by finite differences would be costly in this case. Thus, we propose to use the following QN scheme to get an approximation $\boldsymbol{Q} \approx \boldsymbol{J}$, which exploits certain special structure of this particular problem, namely, sparsity and a known linear part. Assuming the implicit Euler method (20) for time stepping, the exact Jacobian is

$$\begin{aligned}\boldsymbol{J}(\boldsymbol{x}) &= \boldsymbol{A}(\boldsymbol{x}) + (D_{\boldsymbol{x}}\boldsymbol{A}(\boldsymbol{x}))\boldsymbol{x} \\ &= \tfrac{1}{\Delta t}\boldsymbol{M} + \boldsymbol{K} + \boldsymbol{K}^{\mathrm{Fe}}(\boldsymbol{x}) + (D_{\boldsymbol{x}}\boldsymbol{K}^{\mathrm{Fe}}(\boldsymbol{x}))\boldsymbol{x} \\ &= \boldsymbol{J}_{\mathrm{lin}} + \boldsymbol{J}_{\mathrm{Fe}}(\boldsymbol{x})\end{aligned} \tag{24}$$

where $\boldsymbol{J}_{\mathrm{lin}} := (1/\Delta t)\boldsymbol{M} + \boldsymbol{K}$ and $\boldsymbol{J}_{\mathrm{Fe}}(\boldsymbol{x}) := \boldsymbol{K}^{\mathrm{Fe}}(\boldsymbol{x}) + (D_{\boldsymbol{x}}\boldsymbol{K}^{\mathrm{Fe}}(\boldsymbol{x}))\boldsymbol{x}$. Matrix $\boldsymbol{Q}_k$ denotes the approximation of the Jacobian at the kth iteration. The aim is to construct

$$\boldsymbol{Q}_k = \boldsymbol{J}_{\mathrm{lin}} + \tilde{\boldsymbol{Q}}_k \tag{25}$$

such that $\tilde{\boldsymbol{Q}}_k$ retains the sparsity pattern of the exact $\boldsymbol{J}_{\mathrm{Fe}}$. On the first iteration, FP iteration is used, i.e., $\tilde{\boldsymbol{Q}}_k = \boldsymbol{K}^{\mathrm{Fe}}(\boldsymbol{x}_k)$ for

$$k = 0, 1, \ldots, k_{\mathrm{start}} - 1 \tag{26}$$

where the parameter k_{start} is chosen to be 2 or 3 in our simulations. In other words, the term $(D_x\boldsymbol{A})\boldsymbol{x}$ is neglected during the first iterations (another possibility is to store $\tilde{\boldsymbol{Q}}$ from the previous time step). When $k \geq k_{\mathrm{start}}$, $\tilde{\boldsymbol{Q}}_{k+1}$ is updated by the so-called Fletcher's method, a sparse variant of good Broyden's method [8]. The method is modified to detect round-off errors, which could otherwise make the iteration fail. The resulting update formula is

$$\begin{cases} \boldsymbol{q}^l_{k+1} = \boldsymbol{q}^l_k + \frac{y^l - (\boldsymbol{q}^l_k)^T\Delta\boldsymbol{x}}{\sum_j \xi_{i,j}(\Delta\boldsymbol{x}_j)^2}\sum_j \xi_{i,j}\Delta\boldsymbol{x}_j \\ \qquad\qquad \text{if } |\boldsymbol{q}^i_{k+1}\cdot\Delta\boldsymbol{x} - \Delta\boldsymbol{y}_i| < \mathrm{TOL}_{\mathrm{QN}} \\ \boldsymbol{q}^l_{k+1} = \boldsymbol{q}^l_k, \ \text{otherwise} \end{cases} \tag{27}$$

where $\boldsymbol{q}^l_k$ is the lth row of $\tilde{\boldsymbol{Q}}_k$, $\Delta\boldsymbol{x} := \boldsymbol{x}_{k+1} - \boldsymbol{x}_k$, $\boldsymbol{y} := \boldsymbol{K}_{\mathrm{Fe}}(\boldsymbol{x}_{k+1})\boldsymbol{x}_{k+1} - \boldsymbol{K}_{\mathrm{Fe}}(\boldsymbol{x}_k)\boldsymbol{x}_k$, and ξ is the sparsity pattern, i.e., $\xi_{i,j} = 1$ if $\boldsymbol{K}^{\mathrm{Fe}}_{i,j}$ is nonzero, otherwise $\xi_{i,j} = 0$. The if-condition detects "numerical 0/0," which occurs when $\boldsymbol{x}^k$ is close to the actual solution. By a proper implementation, the computational cost of the update (27) is small compared with the construction of $\boldsymbol{K}^{\mathrm{Fe}}$ or the solution of a linear system at each iteration. The derivation of (27) is found in the Appendix.

Some alternatives, or complements, to the QN-method are relaxation [7], the so-called polarization method [14] and line-search methods [2]. However, in the numerical tests, the proposed QN method appears to be fast and robust, so the other methods are not considered in this paper, even though a comparison could be interesting.

V. Implementation

Due to the reasons given in Section II-A, the JA equation (1) is integrated using an adaptive method such that $\Delta\boldsymbol{B}$ is subdivided into s and $2s$ smaller subintervals, and the difference between these two solutions, $\boldsymbol{H}^s$ and $\boldsymbol{H}^{2s}$, is compared. At FE integration points where the (relative) difference is too large, the solution is recomputed using halved step size $4s$, and and this halving is continued until the relative and/or absolute difference is small enough, i.e., at the smallest $m = 0, 1, 2, \ldots$ such that

$$\|\boldsymbol{H}^{2^{m+1}} - \boldsymbol{H}^{2^m}\| < \mathrm{ATOL}_{\mathrm{JA}} \tag{28}$$

and/or

$$\frac{\|\boldsymbol{H}^{2^{m+1}} - \boldsymbol{H}^{2^m}\|}{\|\boldsymbol{H}^{2^{m+1}}\|} < \mathrm{RTOL}_{\mathrm{JA}}\,. \tag{29}$$

In practice, a large number of refinements are required only in a limited number of spatial points, and the location of those points varies during simulation, so it would be inefficient to use some fixed large s at every point (in some cases, one requires $s > 500$ to have stable solution, and it would be unacceptably slow to compute everything with such an accuracy). In our simulations, too large integration error in the JA equation manifests as slowly (or not at all) converging field-equation iterations, and even worse, diverging H–B loops. The adaptive error control seems to solve both of these problems.

With linear elements, we use one quadrature point in each hysteresis element. Thus, we must adaptively solve JA equation once per element per time step per iteration. The value of

TABLE I
JA-MODEL PARAMETERS

	M_s	a	α	k	c
JA1	$1.55 \cdot 10^6$	50	$1.9 \cdot 10^{-6}$	448	0.9
JA2	$1.55 \cdot 10^6$	50	$1.9 \cdot 10^{-6}$	1000	0.5
JA3	$1.55 \cdot 10^6$	50	$1.9 \cdot 10^{-6}$	2000	0.2

$\boldsymbol{H}$ and $\Delta\boldsymbol{H}$ in each element is stored to be the initial values of the next time-step's iteration. With quadratic elements, we use three quadrature points per element. These choices give an exact quadrature for a linear problem and a negligible integration error (compared with other error sources) for a nonlinear problem.

In our test problems, the evaluation of the JA function (1) takes the most of the computation effort, so the routines related to the JA model should be implemented as efficiently as possible. First, the anhysteretic curve (Section II-A) is usually given using the Langevin function $L(x) = \coth(x) - 1/x$, which is expensive to evaluate and values near zero need to be handled separately. For these reasons, the Langevin function is replaced with a fast and once differentiable spline in the implementation. The Langevin function L and its derivative L' are monotonous, and, for example, cubic Hermite spline fits to $L(x_n)$ and $L'(x_n)$, where x_n are the nodes, retains these properties. In addition, the JA-model-related routines (Section II-A) are written in a lower level language (C++) than the rest of the implementation (MATLAB).

Mechanical rotation is included in the FEM by the moving band technique [15], which is implemented so that the "jumps" caused by remeshing are as small as possible. This is achieved by placing the nodes in the moving band slightly asymmetrically and having a different number of nodes on the boundaries, so that the whole moving band triangulation does not change abruptly at certain rotor angles. Large jumps, in addition to other problems, would lead to large $\Delta\boldsymbol{B}$ in the solution of the JA equation, and make its solution more difficult.

The field equation (17) is solved either by FP iteration (22) or the QN scheme (27). The iteration is stopped when the (relative) residual is small enough

$$\frac{\|\boldsymbol{f}(\boldsymbol{x}_k) - \boldsymbol{f}(\boldsymbol{x}_{k-1})\|}{\|\boldsymbol{x}_k\|} < \mathrm{RTOL_{FE}}\,. \tag{30}$$

VI. NUMERICAL TESTS

The simulated device is a 4-pole, 37-kW, 1500-r/min induction machine with a squirrel-cage rotor, rotating at a constant speed (slip 0.01). The field equation is coupled to three-phase voltage supplied stator winding and rotor-cage circuit equations [13]. The supply voltage is initially dampened in such a way that it increases from zero to its steady-state amplitude smoothly; this reduces the initial transient and makes the computation easier without changing the steady-state solution. The domain is one quarter of the machine, where the boundary conditions for A are antiperiodic on the symmetry boundaries and zero Dirichlet condition on the outer boundary.

The JA-parameter set JA1 (see Table I) is used unless otherwise stated. In reality, the core lamination sheets are significantly anisotropic. This is neglected in this paper, which focuses only on the numerical convergence problems, as we expect that including the anisotropy does not change the convergence properties considerably.

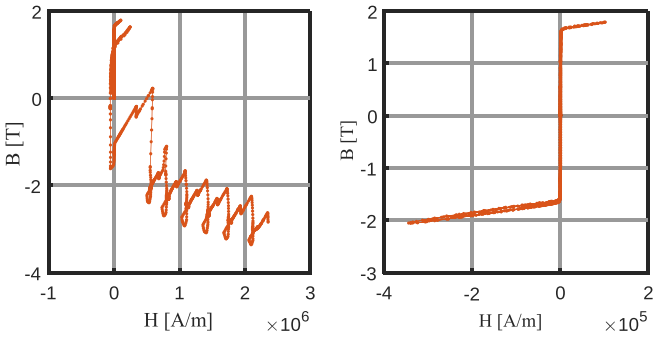

Fig. 2. Simulated H–B curve in the rotor, close to the air gap, tangential component. Left: diverging solution, fixed step size in JA integration. Right: stable solution, adaptive step size.

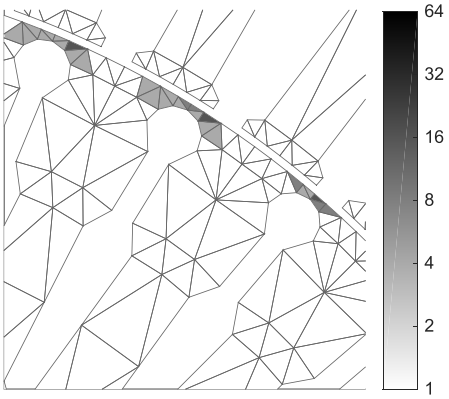

Fig. 3. Number of adaptive JA-integration subdivisions at each iron element. The distribution varies between time steps.

A. Adaptive JA Integration

The simulated H–B curves may diverge if too large error is allowed in the solution of the JA equation. This is illustrated in Fig. 2, which shows a diverging solution (fixed step size without error control, $s = 8$) versus a stable solution (adaptive method, s varies between 2 and 256).

The adaptive method assigns a different number of subdivisions at different elements, which is illustrated in Fig. 3. As expected, the region near the air gap, and especially on the saturating rotor iron bridges, is the most critical, as the change $\Delta\boldsymbol{B}$ per time step is the largest there.

Choosing proper tolerances $\mathrm{ATOL_{JA}}$ and $\mathrm{RTOL_{JA}}$ [see (28) and (29)] appears to be crucial. Too large tolerance leads to diverging solutions, whereas too small tolerance requires a large number of subdivisions when integrating the JA equation, which is the most time-consuming part in our test problems.

B. Comparison of FP and QN Methods

To compare the computational efficiency of the different nonlinear solvers, simulations were run for two-stator voltage source periods using different nonlinear solver methods.

TABLE II
NUMBER OF FIELD-EQUATION ITERATIONS AND COMPUTATION TIME

n_{per}	Single-valued **			Jiles-Atherton **		
	FP	QN	NR	FP	QN	
400	*	*	5.01	*	8.25	Iters/time step
	*	*	41.0	*	187	Comp. time (s)
800	*	13.1	3.72	17.1	4.75	Iters/time step
	*	319	62.3	431	151	Comp. time (s)
1200	*	8.22	3.20	7.73	3.92	Iters/time step
	*	281	80.4	275	175	Comp. time (s)
1600	*	6.34	3.07	4.82	3.50	Iters/time step
	*	274	93.6	340	279	Comp. time (s)

* Does not converge
** Computation times of single-valued v.s. JA should not be directly compared, as JA-functions are optimized on a lower level code.

One source voltage period was divided into n_{per} time steps. The required number of FP, QN, or exact NR (applicable only with the SV H–B model) iterations required to solve the time-stepping field equation (19) is shown in Table II, along with the computation times. Note that the total computation time does not scale linearly with the number of field-equation iterations, because the number of adaptive JA-equation solutions can vary.

The SV H–B case represents a problem where the exact Jacobian is available and the methods are well established. The performance of the QN method is between FP and NR methods, as expected. The FP method converges extremely slowly, if at all. In this case, the QN method does not provide any advantage over the NR method, because the exact Jacobian is easy to compute. However, this demonstrates that the proposed QN method is applicable to a nonlinear FE-equation system.

Using the JA model, the QN method can offer a significant speedup compared with the plain FP method. However, for small time steps ($n_{\mathrm{per}} > 1200$), the performance gap starts to close, as both the methods converge in less than five iterations. It can be beneficial to the computation speed, while not strictly necessary for convergence, to use a smaller time step with the JA model than what is conventionally used with an SV model.

C. Effect of Hysteresis on Stator Current

To "numerically validate" the results, the stator current is computed using an SV iron model and JA with different sets of parameters. The parameter sets (JA1, JA2, and JA3; see Table I) describe either a low-loss (thin loop, JA1) or high-loss material (thicker loop, JA2 and JA3), but they have the same anhysteretic curve (parameters k and c control the thickness of the loop, whereas M_s, a, and α affect only the anhysteretic curve [10] for more physical details). The SV curve in this case is a spline-fitted to minor loops of sinusoidal excitation. It is expected that the quantities computed using the JA model should approach the SV model's results as the JA parameters approach an SV model (i.e., when $k \to 0$, $c \to 1$). The simulation is run for 100 stator source periods, so that a steady state is reached (at least in quantities such as induced currents, torque, and losses).

The peak of a stator winding current in one of the phases is shown in Fig. 4, with the corresponding RMS values. As expected, the values computed using a "thin loop" (JA1 and JA2) are close to the SV results. When the hysteresis loop thickness is increased significantly (JA3), the RMS- and peak values increase by about 10 percent. The parameter set JA1 is probably the closest to a realistic high-grade steel, and in that case one should not expect a large effect on the machine characteristics when the hysteresis is included in the field simulation.

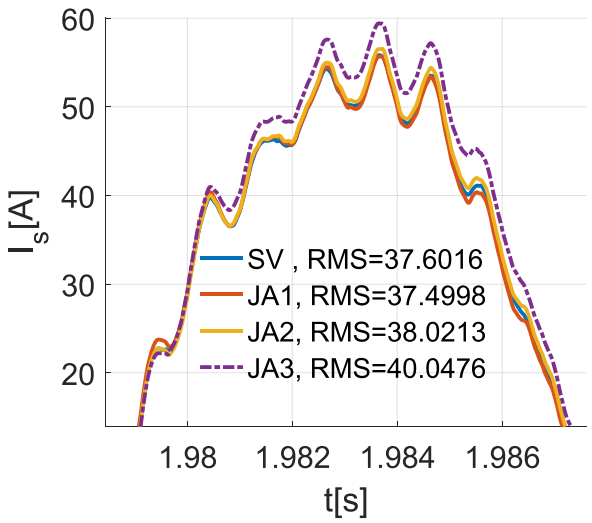

Fig. 4. Simulated stator current, using the SV H–B curve and the JA model with increasing loss terms (see Table I). On this scale, the first three curves are barely distinguishable.

D. Second-Order Elements and Time Integration

For simplicity, the previous numerical tests were executed using the first-order FEs and implicit Euler for time stepping. However, the second-order (quadratic) elements and time integration method (Crank–Nicolson) are usually used in practical simulations. In our tests, the proposed methods appear to work with quadratic elements, but more JA-equation subdivisions are needed, probably because there are more FEM-quadrature points where the JA equation is difficult to solve. This suggests that the adaptive scheme can significantly save computational effort as the number of hysteretic quadrature points is increased.

VII. DISCUSSION

The proposed techniques appear to resolve the numerical convergence problems related to coupled JA-FEM. Unfortunately, there are still issues with the computational cost. To have a numerical scheme that is guaranteed to converge, one may require a small step size in the solution of the JA-equation, and it is difficult to tell a priori what is an optimal tolerance for the JA-model's integration error. The worst-case scenario may require hundreds of steps at thousands of FE-quadrature points to get a stable solution, and such simulation can be thousands of times slower than a corresponding simulation with an SV H–B curve. Fortunately, the JA-equation solutions at different quadrature points are independent of each other, so that part of the computation is trivial

to parallelize, and the remaining part is equivalent to a standard nonlinear FE computation, which is a well-established field, parallel computation included.

There is still room for improvement with the methods presented in this paper. First, the adaptive procedure to solve the JA equation given in this paper may be improved. For example, it could be possible to smoothen the function $\boldsymbol{\nu}_{\mathrm{JA}}$ so that the equation becomes easier to solve, but the solution remains essentially unchanged. Second, the proposed QN scheme could also be improved, as the problem has significant special properties such as sparsity, symmetricity, positive-definiteness, and other possible structure.

This paper focuses only on the numerical issues, and we are not yet in a position to compare the simulations with real measurements. Modeling hysteresis in a real electric machine is challenging, because the lamination sheets are magnetically anisotropic, and they are stacked in such a way that the anisotropy direction changes on every sheet layer. Moreover, the JA model with additional dynamic terms may or may not be an appropriate model for iron at around 50 Hz [16].

Finally, the methods in this paper are "engineering solutions" in the sense that they are given without any mathematical proofs. For a problem with an SV monotonous H–B curve, it is known that the problem is well posed, and the FEM solution converges properly to the actual solution [17]. As per our knowledge, such proofs are not found for the hysteretic case. From a numerical point of view, one should check that the solution to (19) exists and is unique; it is possible that this is not true when the time step Δt is too large, for example.

The planned future work involves modifying the vector JA model in order to properly model magnetization in rotating fields in an anisotropic material. After a satisfying model is constructed, the aim is to measure and test the model with a realistic device.

APPENDIX
SPARSE BROYDEN'S METHOD

The QN method behind (27), sometimes called the sparse Broyden's method or Fletcher's method, was introduced in the 1970s and its properties were studied more rigorously by Marwil [8]. The nonlinear FEM problem in this paper has a certain structure that can be exploited when approximating the Jacobian, so formula (27) is derived here.

The nonlinear equation (19) is solved iteratively and an approximate Jacobian of $\boldsymbol{f}$ at the kth iteration is $\boldsymbol{Q}_k$. The approximation is updated on each iteration such that the following secant condition (i.e., an approximation to a directional derivative) holds:

$$\tilde{\boldsymbol{Q}}_{k+1}(\boldsymbol{x}_{k+1} - \boldsymbol{x}_k) = \boldsymbol{f}_{k+1} - \boldsymbol{f}_k. \tag{31}$$

In our specific problem, the Jacobian is of form $\boldsymbol{J} = \boldsymbol{J}_{\mathrm{lin}} + \boldsymbol{J}_{\mathrm{Fe}}$ [see (24)], where $\boldsymbol{J}_{\mathrm{lin}}$ is a known linear part (including, e.g., coupled circuit equations and regions without iron), so the Jacobian approximation can be expressed as $\tilde{\boldsymbol{Q}}_{k+1} = \boldsymbol{J}_{\mathrm{lin}} + \boldsymbol{Q}_{k+1}$, where $\boldsymbol{Q}_{k+1}$ denotes the nonlinear part to be approximated. The secant condition then simplifies into form

$$\boldsymbol{Q}_{k+1}\Delta\boldsymbol{x} = \boldsymbol{K}^{\mathrm{Fe}}(\boldsymbol{x}_{k+1})\boldsymbol{x}_{k+1} - \boldsymbol{K}^{\mathrm{Fe}}(\boldsymbol{x}_k)\boldsymbol{x}_k =: \Delta\boldsymbol{y}. \tag{32}$$

Equation (32) does not determine $\boldsymbol{Q}_{k+1}$ uniquely, so an additional "minimal change"-condition is imposed

$$\min_{\boldsymbol{Q}_{k+1}\in\mathbb{R}^{N\times N}} \|\boldsymbol{Q}_{k+1} - \boldsymbol{Q}_k\|_F^2 \tag{33}$$

where $\|\boldsymbol{X}\|_F^2 = \sum_{i,j} |\boldsymbol{X}_{i,j}|^2$ is the Frobenius norm. The solution to the quadratic minimization problem (33) with the linear constraint (32), with an additional "numerical safeguard," is

$$\begin{cases} \boldsymbol{q}_{k+1}^i &= \boldsymbol{q}_k^i + \frac{\Delta\boldsymbol{y} - \Delta\boldsymbol{x}}{\|\Delta\boldsymbol{x}\|^2}\Delta\boldsymbol{x}_i \\ & \qquad \text{if } |\boldsymbol{q}_{k+1}^i \cdot \Delta\boldsymbol{x} - \Delta\boldsymbol{y}_i| < \mathrm{TOL}_{\mathrm{QN}} \\ \boldsymbol{q}_{k+1}^i &= \boldsymbol{q}_k^i, \ \text{otherwise} \end{cases} \tag{34}$$

where $\boldsymbol{q}_k^i$ is the ith row of the matrix $\boldsymbol{Q}_k$. The additional if-condition is required to have a numerically stable method, because the update term approaches "$0/0$" as the iteration gets closer to the exact solution, leading to numerical round-off errors starting to dominate in the computation. This can be detected by computing first a "candidate $\boldsymbol{Q}_{k+1}$" and checking the validity of (32) row by row; the equation should hold exactly, and all deviation is due to numerical round-off. The rows where the deviation is above some (relative) tolerance are not updated, and as a result, we get the condition (34).

The known sparsity pattern of $\boldsymbol{Q}_{k+1}$ can be fixed, and the previous derivation remains essentially unchanged. The resulting update formula (27) is used in this paper.

REFERENCES

[1] D. C. Jiles and D. L. Atherton, "Theory of ferromagnetic hysteresis (invited)," *J. Appl. Phys.*, vol. 55, no. 6, pp. 2115–2120, 1984. [Online]. Available: http://dx.doi.org/10.1063/1.333582

[2] C. Guérin, K. Jacques, R. V. Sabariego, P. Dular, C. Geuzaine, and J. Gyselinck, "Using a Jiles–Atherton vector hysteresis model for isotropic magnetic materials with the finite element method, Newton-Raphson method, and relaxation procedure," *Int. J. Numer. Model., Electron. Netw., Devices Fields*, vol. 30, no. 5, p. e2189, 2016. [Online]. Available: http://dx.doi.org/10.1002/jnm.2189

[3] M. E. Mathekga, R. A. McMahon, and A. M. Knight, "Application of the fixed point method for solution in time stepping finite element analysis using the inverse vector Jiles–Atherton model," *IEEE Trans. Magn.*, vol. 47, no. 10, pp. 3048–3051, Oct. 2011.

[4] A. Visintin, *Differential Models of Hysteresis*, vol. 111. Berlin, Germany: Springer-Verlag, 1994.

[5] A. Visintin, "Mathematical models of hysteresis," in *The Science of Hysteresis*, G. Bertotti and I. D. Mayergoyz, Eds. Oxford, U.K.: Academic, 2006, ch. 1, pp. 1–123. [Online]. Available: http://www.sciencedirect.com/science/article/pii/B978012480874450004X

[6] A. Visintin, "Ten issues about hysteresis," *Acta Appl. Math.*, vol. 132, no. 1, pp. 635–647, Aug. 2014. [Online]. Available: https://doi.org/10.1007/s10440-014-9936-6

[7] J. B. Padilha, P. Kuo-Peng, N. Sadowski, and N. J. Batistela, "Vector hysteresis model associated with FEM in a self-excited induction generator modeling," *IEEE Trans. Magn.*, vol. 52, no. 3, Mar. 2016, Art. no. 7000304.

[8] E. Marwil, "Convergence results for Schubert's method for solving sparse nonlinear equations," *SIAM J. Numer. Anal.*, vol. 16, no. 4, pp. 588–604, 1979. [Online]. Available: https://doi.org/10.1137/0716044

[9] J. Gyselinck, P. Dular, N. Sadowski, J. Leite, and J. Bastos, "Incorporation of a Jiles–Atherton vector hysteresis model in 2D FE magnetic field computations: Application of the Newton-Raphson method," *COMPEL-Int. J. Comput. Math. Electr. Electron. Eng.*, vol. 23, no. 3, pp. 685–693, 2004. [Online]. Available: https://doi.org/10.1108/03321640410540601

[10] A. J. Bergqvist, "A simple vector generalization of the Jiles–Atherton model of hysteresis," *IEEE Trans. Magn.*, vol. 32, no. 5, pp. 4213–4215, Sep. 1996.

[11] B. Upadhaya, F. Martin, P. Rasilo, P. Handgruber, A. Belahcen, and A. Arkkio, "Modelling anisotropy in non-oriented electrical steel sheet using vector Jiles–Atherton model," *COMPEL-Int. J. Comput. Math. Electr. Electron. Eng.*, vol. 36, no. 3, pp. 764–773, 2017. [Online]. Available: https://doi.org/10.1108/COMPEL-09-2016-0399

[12] J. B. Padilha, P. Kuo-Peng, N. Sadowski, J. V. Leite, and N. J. Batistela, "Restriction in the determination of the Jiles–Atherton hysteresis model parameters," *J. Magn. Magn. Mater.*, vol. 442, pp. 8–14, Nov. 2017. [Online]. Available: http://www.sciencedirect.com/science/article/pii/S0304885316309337

[13] A. Arkkio, "Analysis of induction motors based on the numerical solution of the magnetic field and circuit equations," Ph.D. dissertation, Dept. Elect. Commun. Eng., Helsinki Univ. Technol., Espoo, Finland, 1987. [Online]. Available: http://lib.tkk.fi/Diss/198X/isbn951226076X/isbn951226076X.pdf

[14] E. Dlala, A. Belahcen, and A. Arkkio, "Locally convergent fixed-point method for solving time-stepping nonlinear field problems," *IEEE Trans. Magn.*, vol. 43, no. 11, pp. 3969–3975, Nov. 2007.

[15] J. P. A. Bastos and N. Sadowski, *Electromagnetic Modeling by Finite Element Methods*. Boca Raton, FL, USA: CRC Press, 2003.

[16] S. E. Zirka, Y. I. Moroz, R. G. Harrison, and K. Chwastek, "On physical aspects of the Jiles–Atherton hysteresis models," *J. Appl. Phys.*, vol. 112, no. 4, p. 043916, 2012. [Online]. Available: http://dx.doi.org/10.1063/1.4747915

[17] M. Feistauer and A. Ženíšek, "Finite element solution of nonlinear elliptic problems," *Numer. Math.*, vol. 50, no. 4, pp. 451–475, Jul. 1986. [Online]. Available: https://doi.org/10.1007/BF01396664